IEEE Access
Multidisciplinary | Rapid Review | Open Access Journal

Received February 6, 2020, accepted March 3, 2020, date of publication March 19, 2020, date of current version March 30, 2020.

Digital Object Identifier 10.1109/ACCESS.2020.2981482

Signal Processing of Coast-Ship Bistatic High-Frequency Surface-Wave Radar Using One-Bit Quantized Measurement

BINGFAN LIU, BAIXIAO CHEN, AND MINGLEI YANG
National Laboratory of Radar Signal Processing, Xidian University, Xi'an 710071, China
Corresponding author: Baixiao Chen (bxchen@xidian.edu.cn)

This work was supported by the National Natural Science Foundation of China under Grant 61571344.

ABSTRACT The feasibility of one-bit quantization in coast-ship bistatic high-frequency surface-wave radar (HFSWR) is mainly discussed in order to enjoy the advantages of simplicity, low cost and low power consumption. Our theoretical derivation shows that the received signal after one-bit quantization can be expressed as a linear combination of infinite components. These components include the original component and the high-order components that can be regarded as the interference terms. Then, the variation of the magnitude of each component with the signal-to-noise ratio (SNR) is given. To reduce the negative impact of these high-order components on the radar system, the detailed signal forms are analyzed. Furthermore, some comparative simulations of one-bit quantization and traditional high-precision quantization are provided to verify the correctness of our theoretical analysis. Both theories and simulation results indicate that the high-order components can be ignored in coast-ship bistatic HFSWR and that one-bit quantization is effective. Finally, real data analysis also validates the efficiency of one-bit quantization in practice.

INDEX TERMS One-bit radar, bistatic high-frequency surface-wave radar, MIMO radar.

I. INTRODUCTION

The coast-ship bistatic high-frequency surface-wave radar (HFSWR) has been capable of playing the irreplaceable role in monitoring the sea surface state and tracking targets with the virtues of low cost and the ability of operation in all weathers [1]. And the coast-ship bistatic HFSWR combines the benefits of high-frequency radar and bistatic radar. Since the receiving station does not radiate energy, the coast-ship bistatic HFSWR has better performance in flexibility, maneuverability and the ability to provide long early warning time [2], [3]. Inspired by the synthetic impulse and aperture radar (SIAR) [4], [5], a novel coast-ship bistatic HFSWR with multiple carrier frequencies has been proposed in [6], [7]. The radar system in [6], [7] employs an array mounted on the coast to simultaneously transmit a set of orthogonal waveforms, and an omni-antenna on a ship to receive echo signals. Thus, this radar system is similar to multiple-input multiple-output (MIMO) radar [8]. By proper processing, an equivalent transmitting pattern is formed with a reception antenna [9].

The associate editor coordinating the review of this manuscript and approving it for publication was Chengpeng Hao.

The most significant advantage of the radar system in [9] is that plenty of ships could share a common transmitting array. There are two potential applications. One is that in the civilian field, a large number of fishing boats can be warned of surrounding non-cooperative dangerous targets, e.g. pirates. The other one is that in the military field, a large number of unmanned boats with small size perform detection jointly in a area close to the enemy targets. The coming challenge is how to reduce equipment costs. Recently, a low-cost radar technology, one-bit quantization technology, has emerged [10], [11]. One-bit quantization refers to a one-bit analog-to-digital Converter. Traditional ADCs have many bits in order to make the signal undistorted. For one-bit quantization, only one bit is used to represent the signal amplitude at a certain time, which means that expensive high-precision ADCs can be replaced with cheaper comparators. And the following advantages can be achieved by one-bit quantization technology. (1) Low cost and low power consumption are conducive to miniaturization of equipment. (2) Comparator is easy to achieve higher rate sampling. (3) One-bit quantized data is beneficial to store and process.

In [12]–[15], processing of synthetic aperture radar (SAR) data coded with one-bit was considered. First of all, basic

processing in SAR, pulse compression or convolution operation, was discussed in detail in spectrum analysis, computation burden, and data storage [12]. Results in [12] show that time-domain convolution between binary sequences allows a mass storage saving with respect to the conventional convolution performed via Fast Fourier Transforms (FFTs), and in several cases also a time saving. Most importantly, when the signal-to-noise ratio (SNR) is low, the matched filter is still effective. Next, the information of SAR raw signal can be restored from the one-bit quantized signal and the image does not exhibit any appreciable degradation [13], [14]. In [15], a SAR platform using one-bit quantization processed binary data in real time with simple, small low-cost and low-power devices.

The effects of one-bit quantization on the direction-of-arrival (DOA) estimation accuracy have also been analyzed in [16]. The corresponding one-bit Cramér-Rao bound (CRB) for a two-sensor array has been derived. Numerical results in [16] show that using one-bit quantization may be an elegant choice for DOA systems and can provide reasonable practical accuracy. However, in essence, one-bit quantization does lose some information and introduce new interferences. In order to get better estimation accuracy, some novel DOA estimation methods have been introduced [17]–[19], such as support vector machine (SVM) based method [17], binary iterative hard thresholding (BIHT) method [18] and Sparse Bayesian Learning (SBL) based method [19]. Classical subspace-based methods, such as multiple signal classification (MUSIC), have been verified to be straightforwardly applied without extra pre-processing [20]. In addition, it is shown in [21] that sparse arrays (nested and coprime arrays) are more robust to the deleterious effects of one-bit quantization, compared to uniform linear arrays (ULAs). For 5G wireless communication system, one-bit ADC has been widely studied in channel estimation, DOA estimation and system performance [22], [23].

Recently, one-bit quantization has once again attracted considerable research interest in radar [10], [24]–[26]. In [10], the conventional radar measurement scheme is replaced by the one-bit sampling with Gaussian and uniform dithering. The one-bit samples can be efficiently processed by using conventional methods proposed for high-precision samples. Sampling with dithering is also known as sampling with time-varying thresholds in [24]–[26]. The problem of sparse parameter estimation with one-bit quantization was considered in [24]. And the CRB for parameters of the single sinusoidal case was computed for a variety of parameter values [25]. Also for one-bit sampling with time-varying thresholds in [26], the target estimation is formulated as a multivariate weighted-least-squares optimization problem that can be solved in a cyclic manner. In [11], one-bit linear frequency modulated continuous wave (LFMCW) radar was studied and a two-stage target detection approach termed as dimension reduction generalized-approximate-message-passing (DR-GAMP) was proposed. It is worth noting that in [10], [11], [24]–[26], there is a common interesting phenomenon: for one-bit quantization, higher SNR does not necessarily lead to better parameter estimation performance.

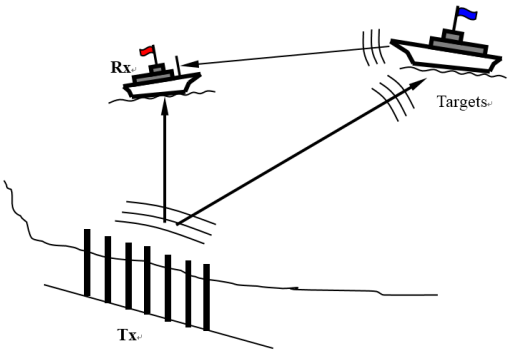

FIGURE 1. Geometry of the coast-ship bistatic HFSWR.

Essentially, the fewer the number of quantization bits, the more distortion the signal has. A natural question is: as an extremely low precision quantization, can one-bit quantization ensure that the information is not lost and the parameter measurement function of coast-ship bistatic HFSWR is not affected? The main goal of this study will answer the question and the main contributions are summarized as follows:

(1) The components of the received one-bit signal in coast-ship bistatic HFSWR are analyzed. One-bit quantization will result in additional high-order components. The variations of these components with respect to SNR are given. It can be found that the lower the SNR, the larger the difference between the average amplitudes of the high-order components and the original components.

(2) The signal forms of high-order components are analyzed. High-order components with different slopes, Doppler information, and distance information from the original component cannot be accumulated in traditional signal processing (e.g. pulse compression, beamforming, and coherent integration).

(3) The feasibility of one-bit in the coast-ship bistatic HFSWR is verified by numerical simulations and analysis of measured data. Traditional processing methods in the coast-ship bistatic HFSWR are verified to be straightforwardly applied. Compared with high-precision quantization, one-bit quantization has almost no loss. Therefore, one-bit quantization has great potential in the coast-ship bistatic HFSWR.

The rest of this paper is organized as follows. In Section II, an overview of the coast-ship bistatic HFSWR system and signal model are introduced. In Section III, the components of the received one-bit signal are analyzed. Then, multi-carrier frequency LFMICW signal processing is developed and detailed in Section IV. Simulation results are provided in Section V, and the measured data is analyzed in Section VI. This paper is concluded in Section VII.

II. SYSTEM OVERVIEW AND SIGNAL MODEL

The geometry of the coast-ship bistatic HFSWR system is illustrated in Fig. 1. The transmitting array (Tx) of the radar

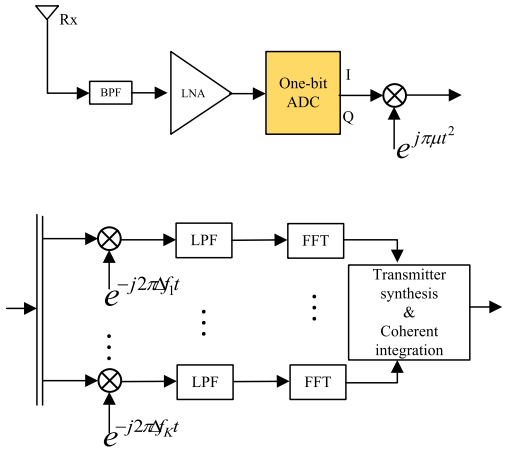

FIGURE 2. Receiver architecture using one-bit quantized measurement.

is a uniform linear array with K antennas, which is placed along the coast. And the receiver system (Rx) with a single antenna is mounted on the boat. The frequency-modulated interruptive continuous waves (FMICW) with multiple carrier frequencies are adopted. The carrier frequencies of transmitting antennas are different from each other, which ensures the orthogonality of the transmitted waveform.

The receiver architecture is illustrated in Fig. 2. Different from high-precision ADCs used in conventional coast-ship bistatic HFSWR, one-bit ADCs are used here. The received signals are filtered, amplified at a low noise level, and sampled at intermediate frequency (IF) by the one-bit ADCs. Other signal processing procedures are consistent with that of the conventional coast-ship bistatic HFSWR with high-precision ADCs. The sampled signals are mixed with the multiple reference signals with the carrier frequencies corresponding to the transmit antennas, and separated through a low-pass filtered (LPF) individually, which is co-called channel separation. After the fast Fourier transform (FFT), i.e., range transforming, the output signal of each channel is obtained. The equivalent transmit beampatterns can be obtained by transmitter synthesis processing. In order to significantly improve target detection performance, it is necessary to perform the coherent integration. Then, we obtain the three basic parameters of target: distance, direction, and speed.

Assuming that f_c is the carrier frequency, the transmitted signal in one sweep period can be expressed by

$$s_k(t) = g(t)\exp(\mathrm{j}2\pi f_k t + \mathrm{j}\pi\mu t^2), \quad 0 \le t \le T,\ k = 1, 2, \cdots, K \tag{1}$$

where K is number of transmit antennas, $f_k = f_c + \Delta f_k$ is the frequency of kth antenna, $\Delta f_k = c_k \Delta f$, $c_k \in \{-(K-1)/2, \ldots, (K-1)/2\}$ is frequency coding, Δf is frequency spacing, $g(t) = \sum_{i=1}^{I} \mathrm{rect}(t - iT_r)$ is the pulse gate signal, $\mathrm{rect}(t) = \begin{cases} 1, & 0 \le t \le T_e \\ 0, & \text{others} \end{cases}$, T_r is the pulse repetition period, T_e is the pulse width, μ is sweep rate, T is sweep period, the sweep bandwidth $B = \mu T$ and I denotes the number of pulse in one sweep period. The time-frequency relationship of the transmitted signal is shown in Fig. 3.

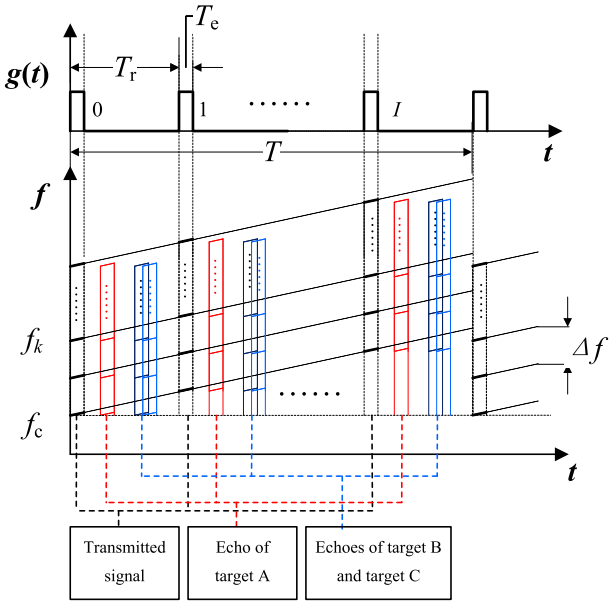

FIGURE 3. Time-frequency relationship of received signal.

The received signal is given by

$$r(t) = \sum_{p=1}^{P}\sum_{k=1}^{K} \beta_p\, s_k(t - \tau_{k,p}) + w(t) \tag{2}$$

where P is the number of targets, $\beta_p = A_p \exp(\mathrm{j}\psi_p)$ is the reflection complex coefficient of the pth target, A_p and ψ_p denote the amplitude and the phase of the complex coefficient, $\tau_{k,p} = (R_p - nv_pT - d_k \sin\theta_p)/c$, $R_p = R_{\mathrm{T},p} + R_{\mathrm{R},p}$ represents the sum of the distance from the transmitting array to the pth target and the distance from the pth target to the receiving array, c is the speed of light, v_p is the equivalent speed of the pth target, d_p is the distance of the kth antenna from the referenced antenna, θ_p is the direction of pth target relative to the transmitting array, and $w(t)$ is complex Gaussian noise with zero mean and covariance $2\sigma_w^2$. In Fig. 3, there are three targets, two of which coincide in the time domain and the remaining one is not affected by other targets.

After one-bit ADC sampling, the received signal can be modeled as

$$\begin{aligned} v(t) &= \mathrm{sign}\{r_{\mathrm{R}}(t)\} + \mathrm{j}\cdot\mathrm{sign}\{r_{\mathrm{I}}(t)\} \\ &= \mathrm{sign}\left\{\sum_{p=1}^{P}\sum_{k=1}^{K} A_p\, g(t-\tau_{k,p})\cos(\Phi_{k,p}(t)) + w_{\mathrm{R}}(t)\right\} \\ &\quad + \mathrm{j}\cdot\mathrm{sign}\left\{\sum_{p=1}^{P}\sum_{k=1}^{K} A_p\, g(t-\tau_{k,p})\cos(\Phi_{k,p}(t) - \frac{\pi}{2}) \right. \\ &\quad \left. + w_{\mathrm{I}}(t)\right\} \end{aligned} \tag{3}$$

where $r_{\mathrm{R}}(t)$ and $r_{\mathrm{I}}(t)$ denote the real and imaginary parts of $r(t)$, $w_{\mathrm{R}}(t)$ and $w_{\mathrm{I}}(t)$ denote the real and imaginary parts of $w(t)$ respectively and sign$(\cdot)$ is signum function. Here, $w_{\mathrm{R}}(t)$ and $w_{\mathrm{I}}(t)$ are Gaussian random variables with zero mean and covariance σ_w^2, and $\Phi_{k,p}$ is written as

$$\begin{aligned}\Phi_{k,p}(t) &= 2\pi f_k(t-\tau_{k,p}) + \pi\mu(t-\tau_{k,p})^2 + \psi_p \\ &\approx 2\pi f_k t + 2\pi f_k(d_k \sin\theta_p/c - \tau_p) \\ &\quad + \pi\mu t^2 - 2\pi\mu t\tau_p + 2\pi f_{\mathrm{d}}^{(p)} nT + \psi_p + \pi\mu\tau_p^2 \quad (4)\end{aligned}$$

where $\tau_p = R_p/c, f_{\mathrm{d}}^{(p)} = f_{\mathrm{c}} v_p/c$ is the Doppler frequency of the pth target.

Noting that sign$(\cdot)$ is a non-linear function. One-bit quantization can no longer guarantee that the received signal is a linear combination of the echoes of different antennas and different targets.

III. ANALYSIS OF ONE-BIT QUANTIZED SIGNAL

A. SIGNAL ANALYSIS FOR ONE TARGET

Without loss of generality, the real part of the received one-bit signal is analyzed. We first consider a segment of the received signal when there is only one target, e.g. the segment where target A is located as shown in Fig. 3. The echo of this target does not overlap with other target echoes, which is the simplest case.

The real part of the received one-bit signal can be expressed in the following integral form [12]

$$\begin{aligned}v_{\mathrm{R}}(t) &= \mathrm{sign}\{r_{\mathrm{R}}(t)\} = -\frac{\mathrm{j}}{\pi}\int_{-\infty}^{\infty}\frac{\exp(\mathrm{j}r_{\mathrm{R}}(t)\xi)}{\xi}\mathrm{d}\xi \\ &= -\frac{\mathrm{j}}{\pi}\int_{-\infty}^{\infty}\frac{\exp(\mathrm{j}w_{\mathrm{R}}(t)\xi)}{\xi} \\ &\quad \times \exp\left\{\mathrm{j}\sum_{k=1}^{K} A_1\cos(\Phi_{k,1}(t))\xi\right\}\mathrm{d}\xi \\ &= -\frac{\mathrm{j}}{\pi}\int_{-\infty}^{\infty}\frac{\exp(\mathrm{j}w_{\mathrm{R}}(t)\xi)}{\xi}\prod_{k=1}^{K} \\ &\quad \times \exp\left\{\mathrm{j}\,A_1\cos(\Phi_{k,1}(t))\xi\right\}\mathrm{d}\xi. \quad (5)\end{aligned}$$

By using the expansion [13]

$$\begin{aligned}&\exp\left\{\mathrm{j}\,A_1\cos(\Phi_{k,1}(t))\xi\right\} \\ &\qquad = \sum_{m=0}^{\infty}\varepsilon_m \mathrm{j}^m J_m(A_1\xi)\cos(m\Phi_{k,1}(t)) \quad (6)\end{aligned}$$

where $\varepsilon_0 = 1$, $\varepsilon_m = 2$ for $m \neq 0$, and $J_m(\cdot)$ is the Bessel function of the first kind, equation (5) can be rewritten as:

$$\begin{aligned}v_{\mathrm{R}}(t) &= -\frac{\mathrm{j}}{\pi}\int_{-\infty}^{\infty}\frac{\exp(\mathrm{j}w_{\mathrm{R}}(t)\xi)}{\xi}\prod_{k=1}^{K} \\ &\quad \left(\sum_{m_{k,1}=0}^{\infty}\varepsilon_{m_{k,1}}\mathrm{j}^{m_{k,1}} J_{m_{k,1}}(A_1\xi)\cos(m_{k,1}\Phi_{k,1}(t))\right)\mathrm{d}\xi \\ &= \sum_{m_{1,1}=0}^{\infty}\sum_{m_{2,1}=0}^{\infty}\cdots\sum_{m_{K,1}=0}^{\infty} \\ &\quad \Omega_{m_{1,1},\cdots,m_{K,1}}\cdot\prod_{k=1}^{K}\cos(m_{k,1}\Phi_{k,1}(t)) \quad (7)\end{aligned}$$

where

$$\begin{aligned}\Omega_{m_{1,1},\cdots,m_{K,1}} &= -\frac{\mathrm{j}}{\pi}\int_{-\infty}^{\infty}\frac{\exp(\mathrm{j}w_{\mathrm{R}}(t)\xi)}{\xi} \\ &\quad \prod_{k=1}^{K}\varepsilon_{m_{k,1}}\mathrm{j}^{m_{k,1}} J_{m_{k,1}}(A_1\xi)\mathrm{d}\xi. \quad (8)\end{aligned}$$

It can be seen from (7) that the original components ($\sum_{k=1}^{K} m_{k,1} = 1$) are preserved after one-bit quantization. Besides, new components ($\sum_{k=1}^{K} m_{k,1} \geq 2$), called high-order harmonics in [9], are generated. Then, we analyze the amplitudes of these new components that could have a negative effect on traditional signal processing. The amplitudes of all components $\{\Omega_{m_{1,1},\cdots,m_{K,1}}\}$ are related to noise w_{R}. The mean of $\Omega_{m_{1,1},\cdots,m_{K,1}}$ with respect to w_{R} is

$$\begin{aligned}&< \Omega_{m_{1,1},\cdots,m_{K,1}} > \\ &= -\frac{\mathrm{j}}{\pi}\int_{-\infty}^{\infty}\int_{-\infty}^{\infty}\frac{1}{\sqrt{2\pi\sigma_w^2}}e^{-\frac{w_{\mathrm{R}}^2}{\sigma_w^2}}\cdot\frac{\exp(\mathrm{j}w_{\mathrm{R}}\xi)}{\xi} \\ &\quad \prod_{k=1}^{K}\varepsilon_{m_{k,1}}\mathrm{j}^{m_{k,1}} J_{m_{k,1}}(A_1\xi)\mathrm{d}\xi\,\mathrm{d}w_{\mathrm{R}} \\ &= -\frac{\mathrm{j}}{\pi}\int_{-\infty}^{\infty}\frac{e^{-\frac{\sigma_w^2\xi^2}{2}}}{\xi}\prod_{k=1}^{K}\varepsilon_{m_{k,1}}\mathrm{j}^{m_{k,1}} J_{m_{k,1}}(A_1\xi)\mathrm{d}\xi. \quad (9)\end{aligned}$$

Let $m = \sum_{k=1}^{K} m_{k,1}$ be the order of the component. By using the equations

$$J_i(x) = J_i(-x) \qquad \text{for } i \text{ being even} \quad (10)$$

$$J_i(x) = -J_i(-x) \qquad \text{for } i \text{ being odd}, \quad (11)$$

$< \Omega_{m_{1,1},\cdots,m_{K,1}} >= 0$ when m is even. Then we focus on the analysis of the case where m is odd. For $K = 1$ or 2, a closed solution to a similar problem has been given in [10]. For $K > 2$, it is difficult to obtain a closed solution of (9). However, we could use Matlab software to calculate $< \Omega_{m_{1,1},\cdots,m_{K,1}} >$ so that we have an understanding of the magnitude of these components.

The SNR is defined as

$$\mathrm{SNR} = \frac{A_p^2}{2\sigma_w^2}. \quad (12)$$

Fig. 4 shows the variation of the main components ($m = 1, 3, 5$) with SNR after one-bit quantization for arrays with different numbers of antennas. The legends '1', '3', '5' in Fig. 4 (a) represent the components $< \Omega_1 >$, $< \Omega_3 >$ and $< \Omega_5 >$ respectively. In Fig. 4 (b), '1-1-1' means that three of $\{m_{k,1}\}_{k=1}^{K}$ are 1, and the rest are 0. '2-3' represents the component $< \Omega_{m_{1,1},\cdots,m_{K,1}} >$ that one of $\{m_{k,1}\}_{k=1}^{K}$ is 2, one is 3, and the rest are 0. By analogy, the meaning of other legends can be derived.

It can be seen from Fig. 4 (b-d) that for components with the same order m, the curves of the amplitude (dB) as a

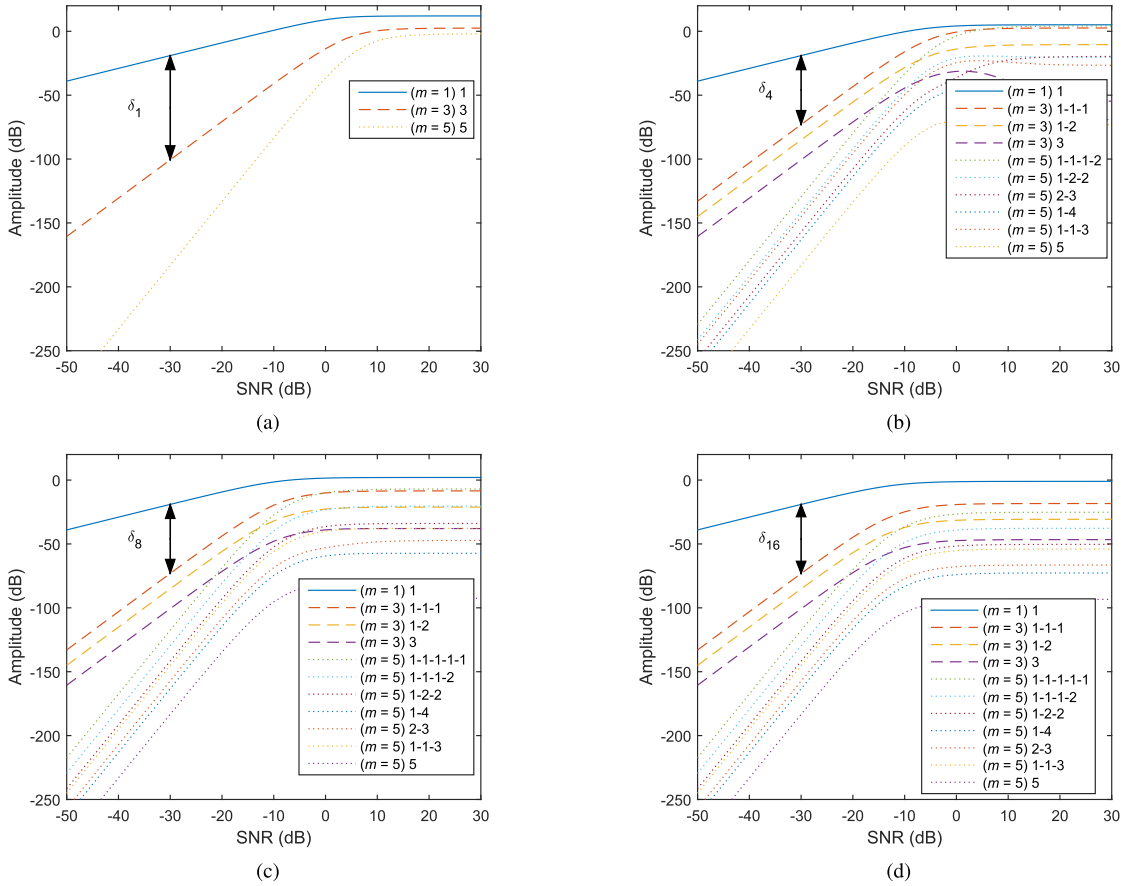

FIGURE 4. Variation of the average amplitudes of the main components ($m = 1, 3, 5$) with the SNR after one-bit quantization for arrays with the number of antennas (a) $K = 1$, (b) $K = 4$, (c) $K = 8$, and (d) $K = 16$.

function of SNR are parallel to each other at a low SNR (dB). In Fig. 4, the solid lines, the dashed lines, and the dotted lines represent first-order, third-order, and fifth-order components, respectively. And the larger the order m, the smaller the component amplitude. And the larger the order m, the smaller the component amplitude. Therefore, there is no further discussion of the components with a large order ($m > 3$). For regions with low SNR, the amplitude difference between the original component ($m = 1$) and the high-order component is large. As SNR increases, all components tend to be flat, and the magnitudes of the high-order components are close to the magnitude of the original component. This phenomenon tells us that one-bit quantization can work well in the case of low SNR, and well explain that the presence of 'ghost scatterers' tend to disappear *as the noise level is increased* in [12], and can also explain that the one-bit Gaussian dithered samples can be processed efficiently by using the conventional algorithm proposed for the infinite precision samples *when noise is sufficiently large* in [10].

Fig. 5 shows the average amplitude difference between the original component and the maximum high-order component. When SNR $= -20$ dB, the maximum high-order component is already 45 dB smaller than the original component.

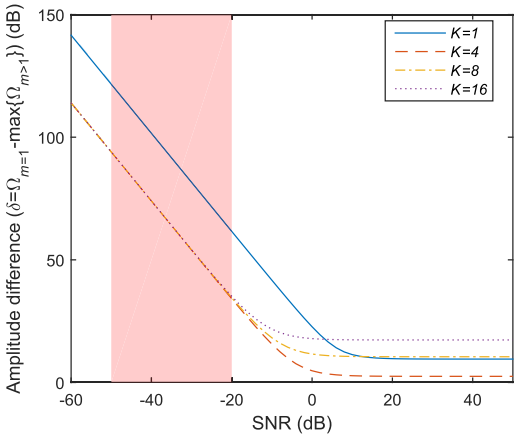

FIGURE 5. Average amplitude difference between the original component and the maximum higher-order component.

For a clearer understanding of high-order components, Fig. 6 shows the time-frequency relationship of one-bit quantized signals with SNR $= 10, -5$ dB when $K = 1$. For $K = 1$, we know from (7) that the possible components are $\cos \Phi_{i,1}$, $\cos 3\Phi_{i,1}$, and $\cos 5\Phi_{i,1}$. Their imaginary parts can be written as $\cos(\Phi_{i,1} - \pi/2)$, $\cos(3\Phi_{i,1} - 3\pi/2)$, and $\cos(5\Phi_{i,1} - 5\pi/2)$, and their complex forms can be written

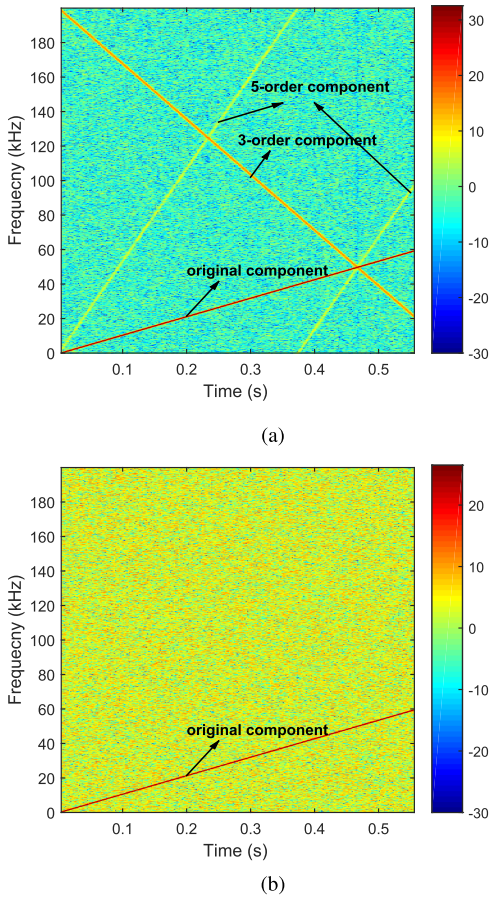

FIGURE 6. Time-frequency relationship of one-bit quantized signal ($K = 1$). (a) SNR = 10 dB, (b) SNR = −5 dB.

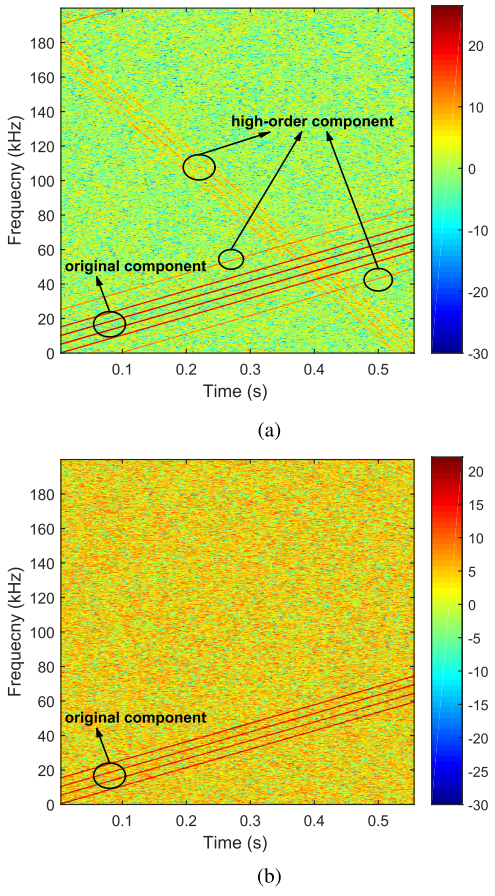

FIGURE 7. Time-frequency relationship of one-bit quantized signal ($K = 4$). (a) SNR = 10 dB, (b) SNR = −5 dB.

as $\exp(\mathrm{j}\Phi_{i,1})$, $\exp(-\mathrm{j}3\Phi_{i,1})$, and $\exp(\mathrm{j}5\Phi_{i,1})$. In Fig. 6 (a), the original component has the highest amplitude. The sweep rate of the 3-order component is negative. The sweep rate of the 5-order component is positive, and due to the limitation of the sampling frequency, the spectrum has an ambiguity phenomenon. The SNR in Fig. 6 (b) is lower, and only the original component can be observed. For $K = 4$, Fig. 7 shows similar results to Fig. 6, except for the more complex high-order components.

In addition, the bandwidths of the high-order components are broadened. The influence of the high-order components on the original components can be further reduced in traditional processing. Taking the 3-order component as an example, the signal forms of the possible components are as follows:

$$\cos 3\Phi_{i,1}\ \cos 2\Phi_{i,1}\cos\Phi_{j,1}\ \cos\Phi_{i,1}\cos\Phi_{j,1}\cos\Phi_{k,1} \quad (1 \le i,j,k \le K) \tag{13}$$

Using the trigonometric identities, the above components (13) can be decomposed into the following components:

$$\begin{aligned}&\text{const},\ \cos\Phi_{i,1},\ \cos 3\Phi_{i,1},\ \cos(2\Phi_{i,1} \pm \Phi_{j,1}),\\ &\cos(\pm\Phi_{i,1} \pm \Phi_{j,1} \pm \Phi_{k,1}) \quad (1 \le i,j,k \le K)\end{aligned} \tag{14}$$

Except for the constant component const and the original component $\cos\Phi_{i,1}$, the other components in (14) can be expressed with the same form:

$$\cos\left(\sum_{i=1}^{3} e_i\Phi_{m_i,1}\right) \quad e_i = \pm 1\ (1 \le m_i \le K) \tag{15}$$

Substituting (4) into (15), we have

$$\begin{aligned}\cos\Bigg(&2\pi\sum_{i=1}^{m} e_i f_{m_i} t + 2\pi\sum_{i=1}^{m} e_i f_{m_i}(d_{m_i}\sin\theta_1/c - \tau_1)\\ &+ \sum_{i=1}^{m} e_i(\pi\mu t^2 - 2\pi\mu t\tau_1 + 2\pi f_{\mathrm{d}}^{(1)} nT + \psi_1 + \pi\mu\tau_1^2)\Bigg).\end{aligned} \tag{16}$$

For the component with $\sum_{i=1}^{m} e_i \ne 1$, the sweep rate is inconsistent with the sweep rate of the original component. Thus, after the dechirp processing, the quadratic term about t cannot be eliminated, and the range transforming can not make this component accumulate.

For the component with $\sum_{i=1}^{m} e_i = 1$, the sweep rate is μ. This component will enter a determinate channel whose frequency $f_{\bar{k}}$ satisfy the condition $f_{\bar{k}} \le \sum_{i=1}^{m} e_i f_{m_i} \le f_{\bar{k}} + \Delta f$. However, since $\sum_{i=1}^{m} e_i\tau_1 = \tau_1$, this component will keep the distance of the target unchanged, which will not cause

interference in the distance dimension. It is worth noting that the azimuth term $2\pi \sum_{i=1}^{m} e_i f_{m_i} d_{m_i} \sin\theta_1/c$ is completely inconsistent with the original azimuth term $2\pi f_{\bar{k}} d_{\bar{k}} \sin\theta_1/c$ of the $\bar{k}$th channel, hence the effects of this components can be negligible on the azimuth dimension.

In summary, the one-bit quantized signal for one target can be processed efficiently by using the conventional algorithm proposed for the infinite precision samples.

B. SIGNAL ANALYSIS FOR TWO OR MORE TARGETS

For multiple targets, the one-bit quantized signal has more complex high-order cross-components. It is assumed that echoes of multiple targets overlap over a certain period of time, e.g., in Fig. 3, the segment where target B and target C are located.

When the equation (7) is extended to $P(P > 1)$ targets, the real part of the one-bit signal can be expressed as

$$v_{\mathrm{R}}(t) = \sum_{m_{1,1}=0}^{\infty} \cdots \sum_{m_{K,1}=0}^{\infty} \cdots\cdots \sum_{m_{1,P}=0}^{\infty} \cdots \sum_{m_{K,P}=0}^{\infty} \Omega_{m_{1,1},\cdots,m_{K,1},\cdots,m_{1,P},\cdots,m_{K,P},} \cdot \prod_{p=1}^{P}\prod_{k=1}^{K} \cos(m_{k,p}\Phi_{k,p}(t)) \tag{17}$$

where

$$< \Omega_{m_{1,1},\cdots,m_{K,P}} > = -\frac{\mathrm{j}}{\pi} \int_{-\infty}^{\infty} \frac{e^{-\frac{\sigma_w^2 \xi^2}{2}}}{\xi} \prod_{p=1}^{P}\prod_{k=1}^{K} \varepsilon_{m_{k,p}} \mathrm{j}^{m_{k,p}} J_{m_{k,p}}(A_p \xi)\mathrm{d}\xi. \tag{18}$$

According to the analysis in Fig. 4, the magnitudes of the 5-order components are much smaller than the magnitudes of the 3-order components. Therefore, we only analyze the 3-order components. When $P = 2$, the 3-order components can be divided into the following three categories:

(1) Self-components of the first target.

$$\cos 3\Phi_{i,1},\ \cos 2\Phi_{i,1}\cos\Phi_{j,1},\ \cos\Phi_{i,1}\cos\Phi_{j,1}\cos\Phi_{k,1} \tag{19}$$

(2) Self-components of the second target.

$$\cos 3\Phi_{i,2},\ \cos 2\Phi_{i,2}\cos\Phi_{j,2},\ \cos\Phi_{i,2}\cos\Phi_{j,2}\cos\Phi_{k,2} \tag{20}$$

(3) Cross-components.

$$\cos 2\Phi_{i,1}\cos\Phi_{j,2},\ \cos\Phi_{i,1}\cos 2\Phi_{j,2}$$
$$\cos\Phi_{i,1}\cos\Phi_{j,1}\cos\Phi_{k,2},\ \cos\Phi_{i,1}\cos\Phi_{j,2}\cos\Phi_{k,2}. \tag{21}$$

Fig. 8 shows the average magnitudes of the components of the two targets as a function of the SNR of target 1. Here, the number of array elements K is 8, and the SNR of the target 2 is set as a constant at -35 dB.

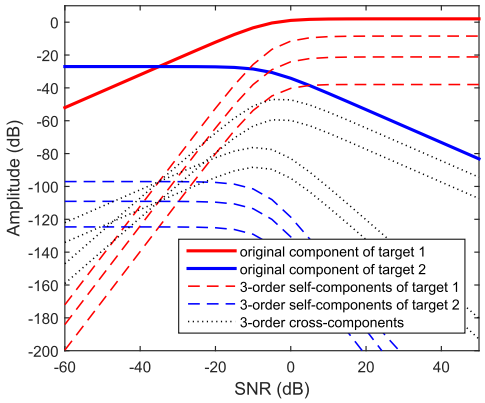

FIGURE 8. Average amplitudes of components of the two targets as a function of the SNR of the target 1, when the SNR of target 2 is constant at −35 dB.

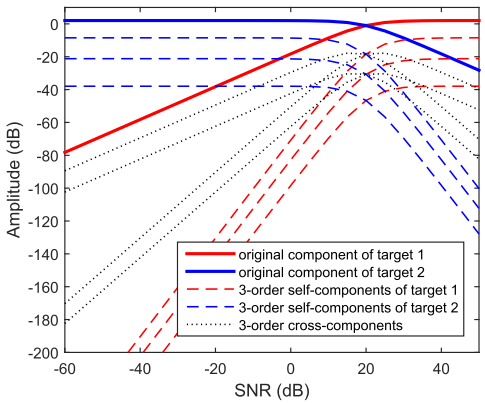

FIGURE 9. The average amplitude of different components of two targets when the SNR of target 2 is constant at 20 dB.

It can be seen that the average amplitude variation of components of target 1 coincides with the average amplitude variation of the component of the single target in Fig. 4 (c). As shown by the solid blue line in Fig 8, the average amplitude of the original component of target 2 remains unchanged as the SNR of target 1 increases when the SNR of target 1 is smaller than −10 dB, but decreases as the SNR of target 1 increases further. It is worth noting that the original component of target 1 gradually approaches the 3-order components of target 2 when the SNR of target 1 is smaller than −60 dB. However, the 3-order self-components of target 2, as described in Section III-A, will not affect traditional processing.

The cross-components of two targets (gray dashed line) always maintain a large gap with the original component of the target 1. At low SNR less than -35 dB, the cross-component with the largest amplitude is parallel to the original component of target 1. When the SNR of target 1 is greater than -35dB, the cross-components will gradually approach the original components.

When the SNR of target 2 is 20 dB, the amplitudes of the components of the two targets varies with the SNR of target 1 as shown in Fig. 9. It can be seen that the amplitude of original components of target 1 are smaller than the

self-components of target 2. According to the analysis in Section III-A, the high-order self-components of target 2 can be suppressed by range transforming. Then, we analyze the cross-components. The signal form of the cross-component with the highest amplitude in Fig. 9 can be described by

$$\begin{aligned}
&\cos\Phi_{i,1}\cos 2\Phi_{j,2}\\
&=\cos(\Phi_{i,1}+2\Phi_{j,2})+\cos(\Phi_{i,1}-2\Phi_{j,2})\\
&=\cos\{2\pi(f_i+2f_j)t+2\pi(f_i(d_i\sin\theta_1/c-\tau_1)\\
&\quad+2f_j(d_j\sin\theta_2/c+2\tau_2))+3\pi\mu t^2-2\pi\mu t(\tau_1+2\tau_2)\\
&\quad+2\pi(f_{\mathrm{d}}^{(1)}+2f_{\mathrm{d}}^{(2)})nT+(\psi_1+2\psi_2)+\pi\mu(\tau_1^2+2\tau_2^2)\}\\
&\quad+\cos\{2\pi(f_i-2f_j)t+2\pi(f_i(d_i\sin\theta_1/c-\tau_1)\\
&\quad-2f_j(d_j\sin\theta_2/c+2\tau_2))+\pi\mu t^2-2\pi\mu t(\tau_1-2\tau_2)\\
&\quad+2\pi(f_{\mathrm{d}}^{(1)}-2f_{\mathrm{d}}^{(2)})nT+(\psi_1-2\psi_2)+\pi\mu(\tau_1^2-2\tau_2^2)\}
\end{aligned}\tag{22}$$

The sweep rate of the first term of (22) is 3μ, thus this term can be ignored in range transforming. And the complex form of the second term of (22) can be written as

$$\begin{aligned}
&\cos(\Phi_{i,1}-2\Phi_{j,2})\\
&\quad+\mathrm{j}\cos((\Phi_{i,1}-\pi/2)-2(\Phi_{j,2}-\pi/2))\\
&=\exp\{\mathrm{j}(2\Phi_{j,2}-\Phi_{i,1})\}\\
&=\exp\{\mathrm{j}2\pi(2f_j-f_i)t+\mathrm{j}2\pi(2f_j(d_j\sin\theta_2/c+2\tau_2)\\
&\quad-f_i(d_i\sin\theta_1/c-\tau_1))-\pi\mu t^2-2\pi\mu t(2\tau_2-\tau_1)\\
&\quad+2\pi(2f_{\mathrm{d}}^{(2)}-f_{\mathrm{d}}^{(1)})nT+(2\psi_2-\psi_1)+\pi\mu(\tau_1^2-2\tau_2^2)\}
\end{aligned}\tag{23}$$

The above equation means that a false target with a Doppler frequency of $(2f_{\mathrm{d}}^{(2)}-f_{\mathrm{d}}^{(1)})$ will appear at $(t=2\tau_2-\tau_1)$, and the angle of this false target cannot be determined from the angle term $\mathrm{j}2\pi(2f_j(d_j\sin\theta_2/c+2\tau_2)-f_i(d_i\sin\theta_1/c-\tau_1))$. Simulations in Section V-C will verify the correctness of this analysis.

For bistatic HFSWR, the direct-path-interference (DPI) can be regarded as a very powerful target with high SNR [9]. If the DPI is not removed completely, the range sidelobes of the DPI will block other targets and the high-order components generated by one-bit quantization will result in false targets. Fortunately, the DPI can be regarded as a target with a high SNR, which allows us to use the traditional method [9] to obtain the precise reference signals and accurately eliminate it.

For multiple targets, high-order components can still be divided into self-components and cross-components. The self-components have the same amplitude distribution as that with only one target in Fig. 4. And the cross-components always have smaller amplitudes than all original components. Their amplitude difference will increase with the decrease of SNR. Therefore, all high-order components can be ignored for coast-ship bistatic HFSWR in an appropriate SNR.

C. SNR IN THE COAST-SHIP BISTATIC HFSWR

We have analyzed the average amplitudes of all components, and we can get a preliminary conclusion that the impact of high-order components can be ignored in a small SNR. However, how small are the SNRs of the targets?

From Fig. 8 and 9, it can be concluded that the high-order cross-components are smaller than the high-order self-component with the highest amplitude (the dotted line is always under the red or blue dashed line). And the amplitude difference between the original component and the maximum high-order self-component is shown in Fig. 5. We assume that the high-order components can be considered to be negligible when the amplitude difference between the original component and the maximum high-order self-component is at least a given value (e.g. 45dB). At this time, the maximum SNR (−20dB) of targets can be determined by the lines in Fig. 5.

The coast-ship bistatic HFSWR has two characteristics. One is the low range resolution, which facilitates long-term coherent integration. The other is employing FMICW, which leads to a high gain of pulse compression. This means that the signal processing gain is high, and the SNR of the target without signal processing can be very low under the given SNR of the target detection. For example, assuming that improvement of SNR in pulse synthesis (the number of the antennas) is $K=16$, the frequency space is 1kHz, the sampling point during the sweep period ($T=0.5$s) is 0.5s ·16kHz = 8000, and the number of coherent integration is 128, the total SNR gain of signal processing is $16\times 8000\times 128=72$dB. If the SNR of the target detection is set to 15dB, the SNR of the unprocessed signal (12) is approximately 15-72 = −57dB. At this time, the high-order components is at least 100dB less than the original component as shown in Fig. 5. Therefore, most targets in the coast-ship bistatic HFSWR meet the application conditions of one-bit quantization.

In summary, there are three reasons why high-order components can be ignored or why one-bit quantization can be applied.

- All types of signals after one-bit quantization bring additional high-order components with lower amplitude. The amplitude differences between the original components and high-order components will increase with the decrement of SNR. Fortunately, unprocessed radar signals generally have a lower SNR.
- With different bandwidth and signal forms from original components, high-order components will be suppressed in the time domain (pulse compression), spatial domain (beamforming), and Doppler domain (coherent integration).
- False targets only appear when the SNR is high, which is rare especially when the DPI is removed.

IV. MULTI-CARRIER FREQUENCY LFMICW SIGNAL PROCESSING

The DPI can be directly set to zero in the time domain, which can eliminate the influence of high-order components

fundamentally. In addition, it is the DPI that we use to extract the reference signals and complete the synthesis processing. Details on DPI removal and synthesis processing have been given in [9].

According to the previous analysis, we can ignore the high-order components. The one-bit quantized signal (3) can be approximated as

$$\begin{aligned} v(n,t) &\approx \sum_{p=1}^{P}\sum_{k=1}^{K}\tilde{A}_p\, g(t-\tau_{k,p})\exp(\mathrm{j}\Phi_{k,p}(t)) \\ &\approx \sum_{p=1}^{P}\sum_{k=1}^{K}\tilde{A}_p e^{\mathrm{j}\psi_p}\, g(t-\tau_{k,p}) e^{\mathrm{j}2\pi f_k t+\pi\mu t^2} \\ &\quad e^{\mathrm{j}2\pi f_k(d_k\sin\theta_p/c-\tau_p)}\cdot e^{-\mathrm{j}2\pi\mu t\tau_p} \\ &\quad e^{\mathrm{j}2\pi f_{\mathrm{d}}^{(p)}nT}\cdot e^{\pi\mu\tau_p^2} \end{aligned} \tag{24}$$

where n represents the index of the sweep period and $\tilde{A}_p$ represents the amplitude of the original component after one-bit quantization. As shown in Fig. 2, $v(n,t)$ is mixed with the referenced signals $\{\exp(\mathrm{j}2\pi f_k t+\pi\mu t^2)\}_{k=1}^{K}$ associated with the transmitting antenna and then are separated through the lowpass filter (LPF) whose output in kth channel is given by

$$\begin{aligned} v_k(n,t) = \sum_{p=1}^{P}\tilde{A}_p e^{\mathrm{j}\psi_p}\cdot e^{\mathrm{j}2\pi f_k(d_k\sin\theta_p/c-\tau_p)} \\ e^{-\mathrm{j}2\pi\mu t\tau_p}\cdot e^{\mathrm{j}2\pi f_{\mathrm{d}}^{(p)}nT}\cdot e^{\pi\mu\tau_p^2} \end{aligned} \tag{25}$$

We convert (25) into range domain by inverse Fourier transform:

$$\begin{aligned} \bar{v}_k(n,\tau) = \sum_{p=1}^{P}\tilde{A}_p e^{\mathrm{j}\psi_p}\cdot e^{\mathrm{j}2\pi f_k(d_k\sin\theta_p/c-\tau_p)}\cdot e^{\mathrm{j}2\pi f_{\mathrm{d}}^{(p)}nT} \\ \frac{\sin[\pi B(\tau-\tau_p)]}{\pi\mu(\tau-\tau_p)} e^{-\mathrm{j}\pi B(\tau-\tau_p)}\cdot e^{\pi\mu\tau_p^2}. \end{aligned} \tag{26}$$

Let $\mathbf{w}(\tau,\theta)=[e^{\mathrm{j}2\pi f_1(d_1\sin\theta/c-\tau)},\cdots,e^{\mathrm{j}2\pi f_K(d_K\sin\theta/c-\tau)}]$ and $\bar{\mathbf{v}}(n,\tau)=[\bar{v}_1(n,\tau),\cdots,\bar{v}_K(n,\tau)]$. The synthesized output is given by

$$\begin{aligned} y(n,\tau,\theta) &= \mathbf{w}^H(\tau,\theta)\bar{\mathbf{v}}(n,\tau) \\ &= \sum_{p=1}^{P}\tilde{A}_p e^{\mathrm{j}\psi_p}\sum_{k=1}^{K} e^{\mathrm{j}2\pi f_k(d_k(\sin\theta_p-\sin\theta)/c-(\tau_p-\tau))} \\ &\quad \frac{\sin[\pi B(\tau-\tau_p)]}{\pi\mu(\tau-\tau_p)} e^{\mathrm{j}2\pi f_{\mathrm{d}}^{(p)}nT}\cdot e^{\pi\mu\tau_p^2}. \end{aligned} \tag{27}$$

Finally, the coherent integration over N number of sweep period, which is also known as Doppler transform, can be implemented by FFT.

It needs to be emphasized again that θ_p denotes the direction of target respect to the transmit array, that the time delay $\tau_p = (R_{\mathrm{T},p}+R_{\mathrm{R},p})/c$ is determined by the sum of the distance from the transmitting array to the pth target and the distance from the pth target to the receiving array, and that $f_{\mathrm{d}}^{(p)}$ is proportional to the derivative of $(R_{\mathrm{T},p}+R_{\mathrm{R},p})$ respect to the time. Therefore, in order to obtain the parameters of the target, coordinate transformation is also required. In this paper, coordinate transformation is the same as that in [6], [9]. We will not discuss it in detail.

V. SIMULATION

In this section, some comparative experiments of one-bit quantization and traditional high-precision quantization to demonstrate the feasibility of one-bit quantization in coast-ship bistatic HFSWR. In all of the following simulations, it is assumed that the transmitting array is ULA with 16 antennas ($K = 16$), the carrier frequency $f_{\mathrm{c}} = 6.75$MHz, the sweep bandwidth $B = 60$kHz, $\Delta f = 1$kHz, the sweep period $T = 0.45$s, $T_r = 3$ms, $T_{\mathrm{e}} = 1$ms, $M = 64$, and the noise power $2\sigma_w^2$ is 1. It is known from the references [7] that the range-azimuth coupling is serious when using sequential carrier frequency distribution. In order to suppress the range-azimuth coupling, we use the optimization method in [7] to obtain the optimal carrier frequencies of antennas:

$$\begin{aligned} \{&-2.5,\ 0.5,\ 6.5,\ -0.5,\ 4.5,\ 3.5,\ -7.5,\ -5.5, \\ &-6.5,\ 5.5,\ -4.5,\ -3.5,\ 7.5,\ 1.5,\ 2.5,\ -1.5\} \\ &\cdot\Delta f + f_{\mathrm{c}}. \end{aligned} \tag{28}$$

A. SIGNAL PROCESSING FOR ONE TARGET

In this example, we consider the case of only one target. This target with SNR of -25 dB and radial velocity of 26.67 m/s is located at the range-azimuth position (320km, 10°). Fig. 10 and 11 show the processing results of high-precision quantization and one-bit quantization. Fig. 10 (a), (b) and (c) show the range-azimuth profile, Doppler-azimuth profile, and Doppler-range profile using the traditional high-precision quantization. Correspondingly, the processing results using one-bit quantization are shown in Fig. 11. It can be seen that the peaks of both results are at the same location. For ease of comparison, Fig. 12 (a), (b) and (c) show the results of one-dimensional processing on range, azimuth, and Doppler frequency. In each dimension, the sidelobes for one-bit quantization and high-precision quantization are approximately consistent. As expected, large peaks exist at the position corresponding to target range, azimuth and Doppler frequency. In the result of one-bit quantization, the most worrying false target did not appear. This means that at low SNR, high-order components are negligible after signal processing.

B. SIGNAL PROCESSING FOR MULTIPLE TARGETS

We consider multiple targets in this experiment, and the parameters of targets are given in Table 1. Here, we assume that all targets are in the same Doppler channel. Fig. 13 shows the range-azimuth profile of one-bit quantization and high-precision quantization. The target positions of the two quantization methods are the same.

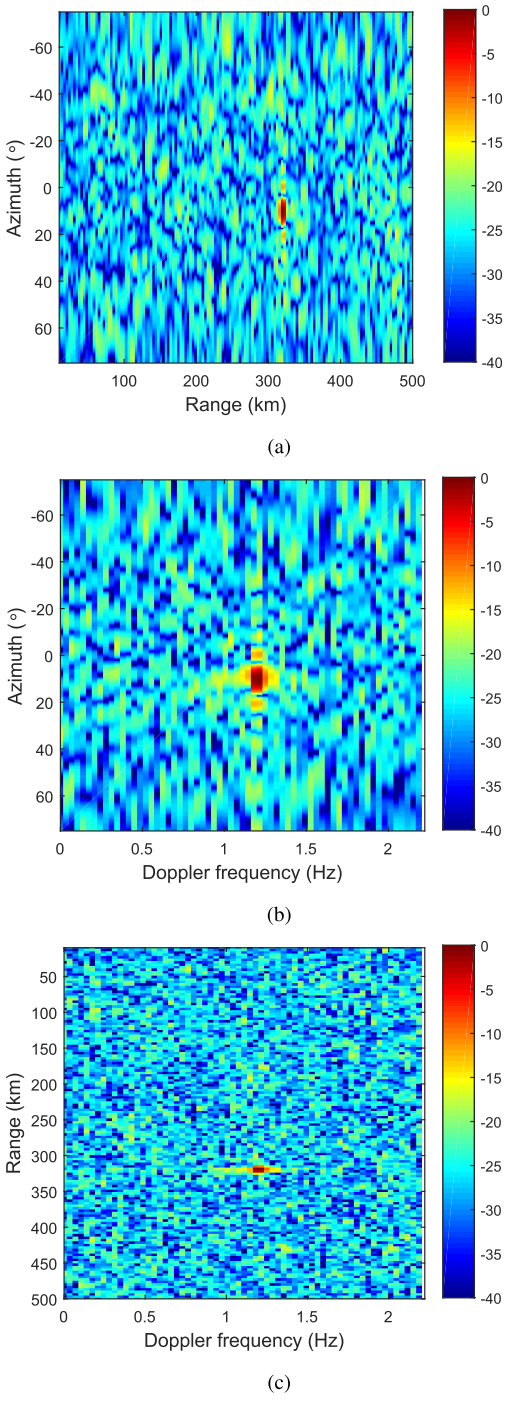

FIGURE 10. Processing results of infinite precision quantization with target SNR of −25dB, range of 320km, angle of 10° and velocity of 26.7 m/s. (a) Range-angle profile. (b) Doppler-azimuth profile. (c) Doppler-range profile.

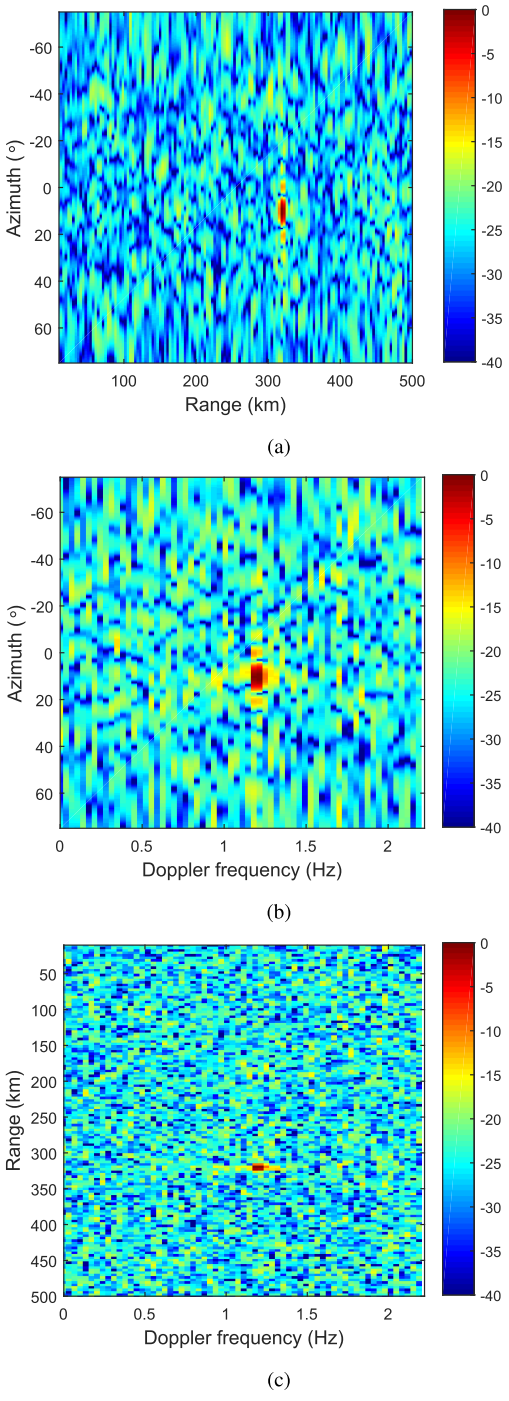

FIGURE 11. Processing results of one-bit quantization with target SNR of −25dB, range of 320km, angle of 10° and velocity of 26.7 m/s. (a) Range-angle profile. (b) Doppler-azimuth profile. (c) Doppler-range profile.

C. FALSE TARGET

In order to verify the correctness of the analysis on the false targets generated by the cross-components, the case of two targets with high SNR is considered. Our analysis in Section III shows that the false targets will only exist in the case of high SNR, and that the SNR of the coast bistatic HFSWR is generally low. Thus, the simulation in this subsection is only to prove the correctness of our theoretical analysis.

The SNR, azimuth, range, and radial velocity of the first target are set to 0dB, −20°, 200km, 0.22 m/s, respectively. The other target with SNR of 10 dB and radial velocity of 0 m/s is located at the range-azimuth position (230km, 30°). The Doppler frequencies of the two targets are 0Hz,

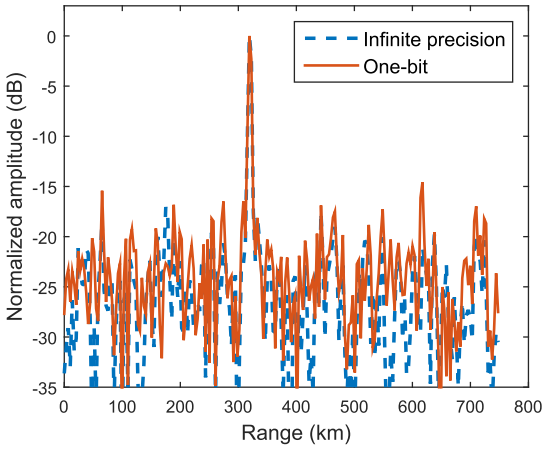

(a)

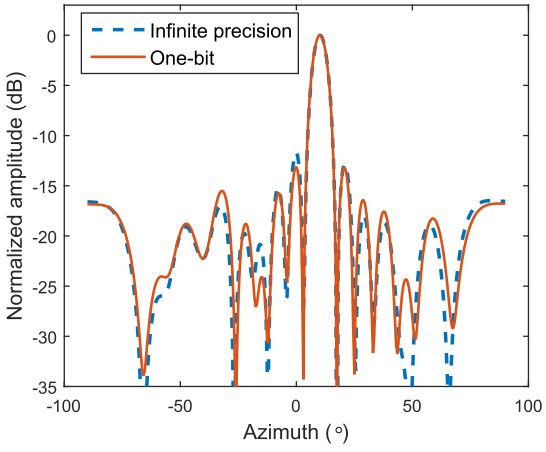

(b)

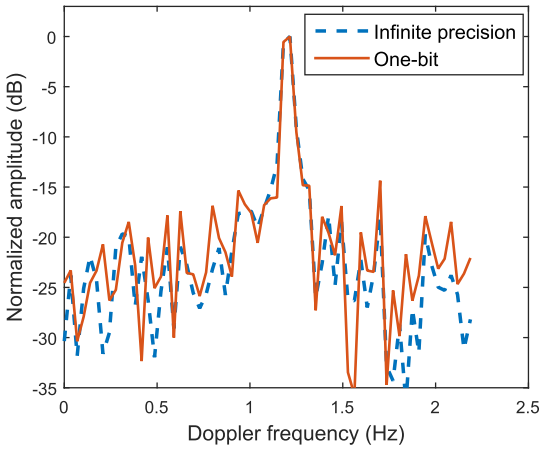

(c)

FIGURE 12. Comparison of output results with infinite precision quantization and one-bit quantization. (a) Range dimension, (b) Azimuth dimension, (c) Doppler frequency dimension.

0.01Hz, thus they are all in the first Doppler channel. The echoes of the two targets overlap by 90%.

Fig. 14 shows the range-azimuth profile of the first Doppler channel. It can be seen that the processing result of one-bit quantization has a false target at 260 km. This result supports

TABLE 1. The parameters of each targets.

Target index	Range(km)	Azimuth (°)	SNR (dB)	Velocity (m/s)
1	343	-35	-32	
2	122	-9	-30	
3	559	23	-30	
4	627	51	-30	4.44
5	597	-58	-30	
6	566	42	-34	
7	115	31	-35	

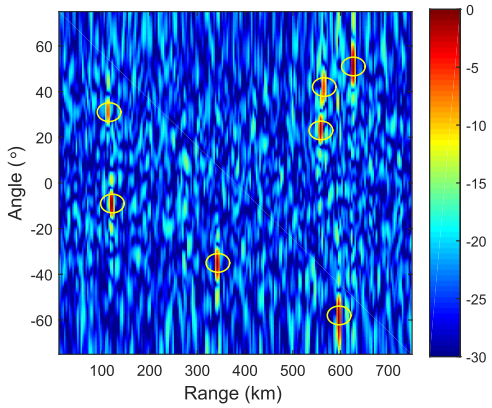

(a)

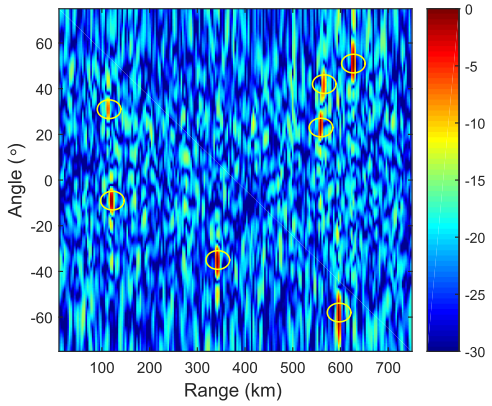

(b)

FIGURE 13. Range-azimuth angle profile when there are 7 targets. (a) Infinite precision quantization, (b) One-bit quantization.

the conclusion in Section III-B that the false target appears at $(230 \times 2 - 200 = 260)$ km.

As analyzed in Section III-C, the SNRs of targets in the coast-ship bistatic HFSWR are usually very low (SNR$\ll$0dB). As a result, false targets will hardly appear in the coast-ship bistatic HFSWR. In the next section, some measured data will confirm this.

VI. MEASURED DATA VALIDATION

In order to verify the effect of one-bit quantization in practice, some measured data collected from a coast-ship bistatic HFSWR are analyzed. This radar system using 14-bit quantization has been introduced in [6], [9]. The transmit array of this radar consist of 8 individual three-element Yagi-Uda

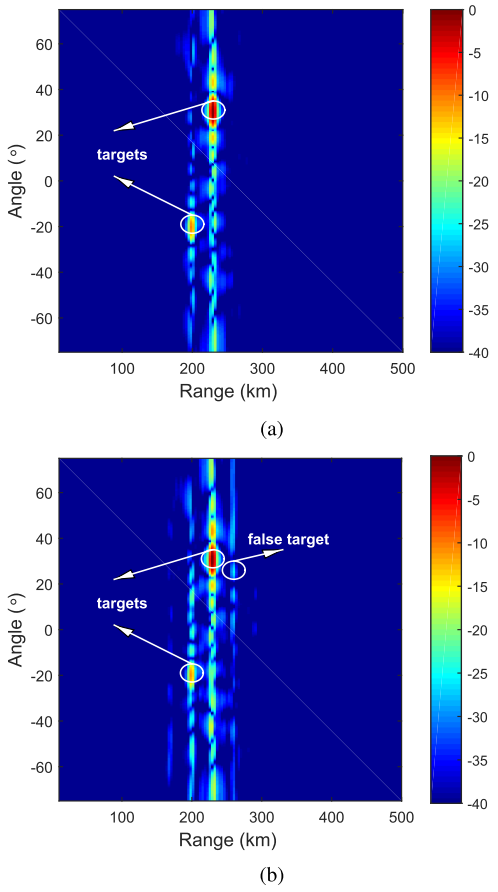

FIGURE 14. Range-azimuth angle profile when two targets with SNR of (0 dB, 10 dB) are located at (200km, −20°) and (230km, 30°) respectively. (a) Infinite precision quantization, (b) One-bit quantization.

FIGURE 15. Transmit array.

antennas as shown in Fig. 15. The Yagi-Uda antenna is composed of 3 elements, a guiding antenna, an active antenna, and a reflecting antenna. Fig. 16 shows the receive antenna placed on a moving boat, which is an isotropic vertical monopole. The carrier frequency $f_c = 6.75$MHz, the sweep bandwidth

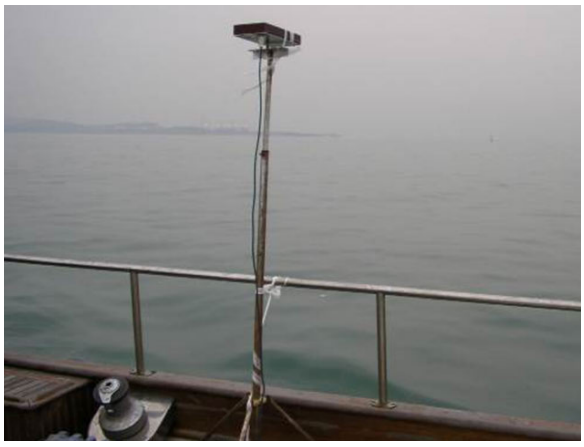

FIGURE 16. Receive antenna.

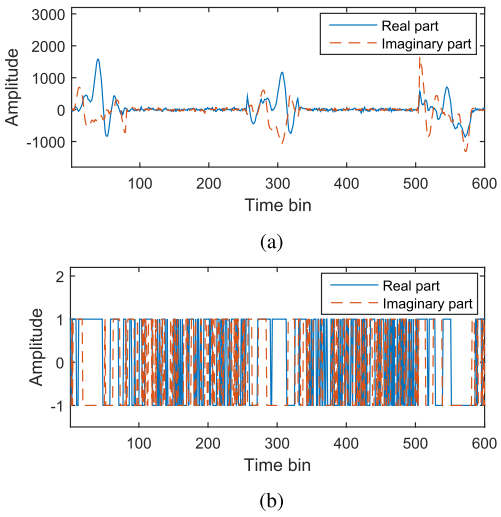

FIGURE 17. Measured I/Q two channel digital signal. (a) 14-bit quantization, (b) One-bit quantization.

$B = 60$kHz, $\Delta f = 3.75$kHz, and the sweep period $T = 0.5$s, $T_r = 1$ms, $T_e = 300\mu$ s.

For comparison, one-bit quantized data is obtained by one-bit resampling of high-precision quantized data. Fig. 17 (a) shows 14-bit quantized data of three sub-pulses. Fig. 17 (b) is the corresponding one-bit quantized data. We can see that the DPI is very clear and its SNR is much greater than 0 dB.

Since the gain of coherent integration in this radar system is much larger than that of synthesis processing, the coherent integration may be prior to synthesis processing (equivalent transmit beamforming). The range-Doppler profile in the first channel is shown in Fig. 18. The results for the other 7 channels are similar to Fig. 18 and are not given here. The number of coherent integration is 512, i.e., the integration time is $512 \times 0.5 = 256$ s. It can be seen from Fig. 18 (a) and (b) that we obtain similar results including sea clutter and several non-cooperative targets. These targets are passing ships on the sea. The slices of the synthesis processing in the range-Doppler units of the four distinct targets are shown in

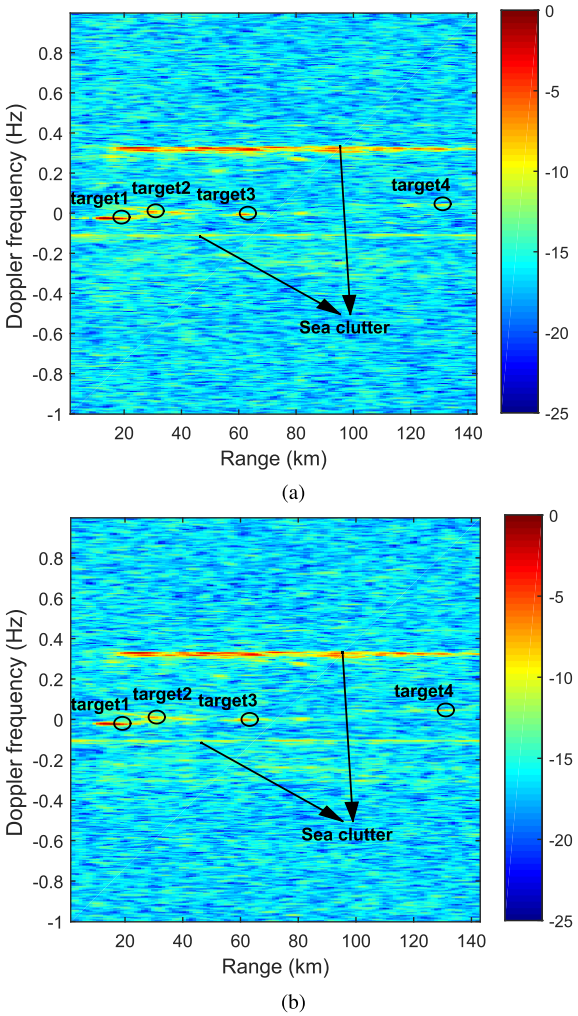

FIGURE 18. Range-Doppler profile of the first channel. (a) 14-bit quantization, (b) One-bit quantization.

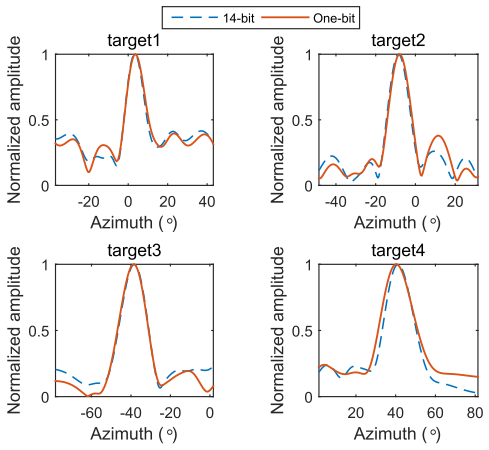

FIGURE 19. Azimuths of targets relative to transmitting station.

Fig. 19. Each target is normalized with its maximum value. Obviously, the accuracy of one-bit quantized data can be comparable to that of high-precision quantized data.

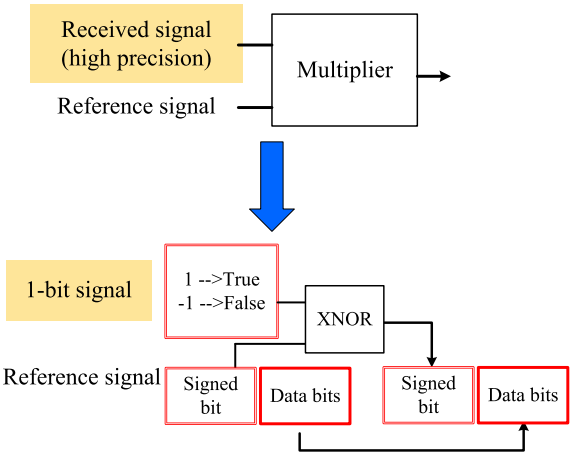

FIGURE 20. Implementation of multiplication of one-bit signal.

Two advantages can be obtained by using one bit quantization in this radar system: reduced data storage and reduced computation of signal processing. In the original radar system, the 14-bit ADC was used and the storage type was 16-bit signed integer. If one-bit quantization is used, the data storage is reduced by a factor of 16. In Fig. 2, the multiplication operation involved in channel separation can be converted into the XNOR operation. As shown in Fig. 20, we perform the XNOR operation on the sign bit of the reference signal and the one-bit quantized data to obtain a new sign bit, and then recombine the new sign bit with the data bits of the reference signal to obtain the product of the reference signal and the one-bit quantized signal.

VII. CONCLUSION

We introduce one-bit quantization into coast-ship bistatic HFSWR to gain many advantages of one-bit quantization, such as low cost and low power consumption. Our theoretical analysis shows that one-bit quantization does not completely distort the original signal, but retains the original component while introducing other high-order components. The magnitudes of these high-order components are generally smaller than that of the original components. After pulse compression, the influence of these high-order components will be further reduced. Numerical simulations and analysis of measured data show that traditional processing methods in the coast-ship bistatic HFSWR are verified to be straightforwardly applied.

In addition, all radars have an important process, pulse compression, which can accumulate the original components and filter out the high-order components, then reduce the adverse impact of one-bit quantization. Even at high SNR, as long as the transmitting waveform and matched filter are properly designed, the influence of high-order components can be reduced. Thus, we will extend one-bit quantization to other radars and our future work will focus on the design of the transmitted waveform and pulse filter to reduce the impact of high-order components caused by one-bit quantization.

REFERENCES

[1] J. M. Headrick and J. F. Thomason, "Applications of high-frequency radar," *Radio Sci.*, vol. 33, no. 4, pp. 1045–1054, 1998.

[2] M. Lesturgie, "Use of STAP techniques to enhance the detection of slow targets in shipborne HFSWR," in *Proc. Int. Conf. Radar*, Aug. 2003, pp. 504–509.

[3] J. Xie, Y. Yuan, and Y. Liu, "Super-resolution processing for HF surface wave radar based on pre-whitened MUSIC," *IEEE J. Ocean. Eng.*, vol. 23, no. 4, pp. 313–321, Oct. 1998.

[4] C. Baixiao, L. Hongliang, and Z. Shouhong, "Long-time coherent integration based on sparse-array synthetic impulse and aperture radar," in *Proc. CIE Int. Conf. Radar*, Beijing, China, Oct. 2001, pp. 1062–1066.

[5] C. Duofang, C. Baixiao, and Z. Shouhong, "Multiple-input multiple-output radar and sparse array synthetic impulse and aperture radar," in *Proc. CIE Int. Conf. Radar*, Shanghai, China, Oct. 2006, pp. 1–4.

[6] C. B. Liu, B. X. Chen, and S. H. Zhang, "Co-channel interference suppression by time and range adaptive processing in bistatic high-frequency surface wave synthesis impulse and aperture radar," *IET Radar Sonar Navig.*, vol. 3, no. 6, pp. 638–645, 2009.

[7] H. Su, H. Liu, P. Shui, S. Zhang, and Z. Bao, "HFSWR based on synthetic impulse and aperture processing," *IEE Proc.-Radar, Sonar Navigat.*, vol. 153, no. 5, pp. 445–453, 2006.

[8] J. Li and P. Stoica, "MIMO radar with colocated antennas," *IEEE Signal Process. Mag.*, vol. 24, no. 5, pp. 106–114, Sep. 2007.

[9] C. Baixiao, C. Duofang, Z. Shouhong, Z. Hao, and L. Maocang, "Experimental system and experimental results for coast-ship Bi/multistatic ground-wave over-the-horizon radar," in *Proc. CIE Int. Conf. Radar*, Shanghai, China, Oct. 2006, pp. 1–5.

[10] J. Ren and J. Li, "One-bit digital radar," in *Proc. 51st Asilomar Conf. Signals, Syst., Comput.*, Pacific Grove, CA, USA, Oct. 2017, pp. 1142–1146.

[11] B. Jin, X. Zhang, B. Zhao, and G. Wu, "One-bit LFM pulse radar: Harmonic analysis and target reconstruction," *IEEE Access*, vol. 7, pp. 109482–109494, 2019.

[12] G. Alberti, G. Schirinzi, G. Franceschetti, and V. Pascazio, "Time-domain convolution of one-bit coded radar signals," *IEE Proc. F, Radar Signal Process.*, vol. 138, no. 5, pp. 438–444, Oct. 1991.

[13] G. Franceschetti, V. Pascazio, and G. Schirinzi, "Processing of signum coded SAR signal: Theory and experiments," *IEE Proc. F, Radar Signal Process.*, vol. 138, no. 3, pp. 192–198, Jun. 1991.

[14] G. Cappuccino, G. Cocorullo, P. Corsonello, and G. Schirinzi, "Real-time processing of one-bit-coded SAR data," in *Proc. 8th Medit. Electrotech. Conf. Ind. Appl. Power Syst., Comput. Sci. Telecommun. (MELECON)*, Bari, Italy, vol. 1, 1996, pp. 117–119.

[15] V. Pascazio and G. Schirinzi, "Synthetic aperture radar imaging by one-bit coded signals," *Electron. Commun. Eng. J.*, vol. 10, no. 1, pp. 17–28, Feb. 1998.

[16] O. Bar-Shalom and A. J. Weiss, "DOA estimation using one-bit quantized measurements," *IEEE Trans. Aerosp. Electron. Syst.*, vol. 38, no. 3, pp. 868–884, Jul. 2002.

[17] Y. Gao, D. Hu, Y. Chen, and Y. Ma, "Gridless 1-b DOA estimation exploiting SVM approach," *IEEE Commun. Lett.*, vol. 21, no. 10, pp. 2210–2213, Oct. 2017.

[18] L. Jacques, J. N. Laska, P. T. Boufounos, and R. G. Baraniuk, "Robust 1-Bit compressive sensing via binary stable embeddings of sparse vectors," *IEEE Trans. Inf. Theory*, vol. 59, no. 4, pp. 2082–2102, Apr. 2013.

[19] X. Meng and J. Zhu, "A generalized sparse Bayesian learning algorithm for 1-bit DOA estimation," *IEEE Commun. Lett.*, vol. 22, no. 7, pp. 1414–1417, Jul. 2018.

[20] X. Huang and B. Liao, "One-bit MUSIC," *IEEE Signal Process. Lett.*, vol. 26, no. 7, pp. 961–965, Jul. 2019.

[21] C.-L. Liu and P. P. Vaidyanathan, "One-bit sparse array DOA estimation," in *Proc. IEEE Int. Conf. Acoust., Speech Signal Process. (ICASSP)*, New Orleans, LA, USA, Mar. 2017, pp. 3126–3130.

[22] Y. Li, C. Tao, G. Seco-Granados, A. Mezghani, A. L. Swindlehurst, and L. Liu, "Channel estimation and performance analysis of one-bit massive MIMO systems," *IEEE Trans. Signal Process.*, vol. 65, no. 15, pp. 4075–4089, Aug. 2017.

[23] L. Fan, S. Jin, C.-K. Wen, and H. Zhang, "Uplink achievable rate for massive MIMO systems with low-resolution ADC," *IEEE Commun. Lett.*, vol. 19, no. 12, pp. 2186–2189, Dec. 2015.

[24] C. Gianelli, L. Xu, P. Stoica, and J. Li, "One-bit compressive sampling with time-varying thresholds for sparse parameter estimation," in *Proc. IEEE Sensor Array Multichannel Signal Process. Workshop (SAM)*, Rio de Janerio, Brazil, Jul. 2016, pp. 1–5.

[25] C. Gianelli, L. Xu, and J. Li, "One-bit compressive sampling with time-varying thresholds: Maximum likelihood and the Cramér–Rao bound," in *Proc. 50th Asilomar Conf. Signals, Syst. Comput.*, Pacific Grove, CA, USA, 2016, pp. 399–403.

[26] A. Ameri, A. Bose, J. Li, and M. Soltanalian, "One-bit radar processing with time-varying sampling thresholds," *IEEE Trans. Signal Process.*, vol. 67, no. 20, pp. 5297–5308, Oct. 2019.

BINGFAN LIU received the B.S. degree from Xidian University, in 2015, where he is currently pursuing the Ph.D. degree with the National Laboratory of Radar Signal Processing. His research interests include signal processing, parameter estimation, MIMO radar, and array signal processing.

BAIXIAO CHEN was born in Anhui, China, in 1966. He graduated from the Metallurgy College of East China, in 1987, and the master's degree in circuit and system and the Ph.D. degree in signal and information processing from Xidian University, in 1994 and 1997, respectively. He was with the Metallurgy College of East China, from 1987 to 1991. He was a Lecturer and an Associate Professor, from 1997 to 1999 and from 1996 to 2003, respectively. Since 1997, he has been a Faculty Member with the National Laboratory of Radar Signal Processing. In 2006, he was selected into New Century elitist Support Program of the Ministry of Education. He is currently a Professor of signal and information processing. His current research interests include radar signal processing, new radar system design, array signal processing, and precise guidance.

MINGLEI YANG received the B.E. degree in electronic engineering and the Ph.D. degree in signal and information processing from Xidian University, China, in 2004 and 2009, respectively. Since 2009, he has been with the National Laboratory of Radar Signal Processing, Xidian University. From 2014 to 2015, he was a Visiting Scholar with the Elisha Yegal Bar-Ness Center for Wireless Communications and Signal Processing Research, New Jersey Institute of Technology. He is currently a Professor in signal and information processing. He has published more than 60 peer-reviewed journals and conference papers, and more than 40 inventions. His research interests include array signal processing, MIMO signal processing, and polarization information processing.